# CLOUDINESS VALIDATION IN THE ECMWF MODEL

Nils Gunnar Kvamstø
European Centre for Medium-Range Weather Forecasts
Shinfield Park, Reading, UK

## 1. INTRODUCTION

In *Morcrette et al.* (1991) radiation and cloud interaction processes are addressed. It was recognized that the present cloud scheme showed limited skill in providing the radiation scheme with realistic cloud distribution and optical properties of the cloud fields.

On this background a new, fully prognostic parametrisation scheme for cloud- and cloud associated processes in the ECMWF model has been developed by *Tiedtke* (1993).

In this report a synoptic validation of the performance of the present operational and the new scheme will be done. Hopefully such a comparison will reveal differences between the schemes and through these show to which extent the new scheme represents an improvement. The investigation is also an attempt to provide information of how any deficiencies of the schemes may be linked to the large scale flow.

The (verification) datasets available for a synoptic day to day validation of cloudiness are infrared satellite imageries and conventional synop observations. Apparently, a more precise and quantitative validation may be carried out by calculating model radiances in the satellite channels and comparing them with the measured radiances. However any differences between the two radiance fields may be due to: a) Unrealistic cloud cover. b) Unrealistic optical properties. c) Unrealistic vertical distribution of clouds. d) Deficiencies in the parametrisation of radiative transfer in clouds. Hence it is advantageous to compare model cloudiness with clouds "retrieved" from satellite radiances as well as radiances directly. Such a validation may help to reduce the ambiguity of any quantitative comparison. The disadvantages of a synoptic validation are that global mean and time integral properties will not be addressed.

Two winter cases over Europe have so far been selected for the cloud validation; 15 - 18 January and 14 February. In addition, some summer cases will be investigated shortly. In the next sections some preliminary results will be presented. The examples are taken from the January period.

## 2. THE CLOUD SCHEMES

Both schemes allow clouds to be present in any model layer but the lowest.

The operational cloud scheme is entirely diagnostic, i.e. it is the cloud fraction itself that is parametrised. Cloudiness associated with convection (cumulus clouds and anvil cirrus) is a function of the scaled time

averaged precipitation rate. The stratiform cloud fraction is mainly a function of relative humidity. Inversion cloudiness is expressed in terms of the vertical temperature gradient and relative humidity. A detailed description of the scheme is given in *Slingo* (1987).

The new scheme introduces the fractional cloud cover as a prognostic variable, which means that it is the sinks and sources of cloud mass that are parametrised instead of the cloud fraction itself:

$$\frac{\partial a}{\partial t} = A(a) + \sum_i S_i \qquad (1)$$

where $A$ denotes the advective terms and $S_i$ denotes the sources and sinks. The form of $S_i$ depends on which process is dominant. For further details see *Tiedtke* (1993). It should be mentioned that experiments with the new scheme investigated in this paper has been performed with no advection (i.e. the A terms are set to zero).

## 3. A SYNOPTIC ASSESSMENT OF THE OPERATIONAL CLOUDINESS FORECAST OVER EUROPE 15-18 JANUARY 1993

Datasets available for such a validation are infrared satellite imageries from Meteosat and conventional synop observations. Those data are available 00, 06 12 and 18UTC each day in the selected period. The observation times is chosen to correspond to the 36, 42, 48 and 54h forecast, respectively. During this period a lot of baroclinic activity took place over the selected area.

### 3.1 **Frontal clouds**

The cloud belts in a mature cyclonic system are associated with the general isentropic motion within the cyclone. In the frame of reference moving with the system, well defined airflows appear. The ascending airflows are often referred to as conveyor belts. Schematically, the warm conveyor belt (WCB) is formed as air originating at lower levels in the warm sector equatorward of the surface low, rises as it flows along the cold front and splits into two branches, one cyclonic and one anticyclonic. This region is often referred to as the "hammer head". Condensation occurs as the warm sector branch is rising, thereby triggering cloud formation and enhancing cross isentropic motion. Thus, WCB is the primary cloud producing flow. Another well defined cloud and precipitation producing flow of this kind is the cold conveyor belt (CCB), often not as distinct and extensive as the WCB. Originating in the anticyclonic low level flow to the north east of the cyclone, the air in the CCB travels westward (relative to the eastward moving cyclone) just ahead of the warm front undercutting the WCB and moves along the back-bent warm front (occlusion). For a more complete and detailed description see *Browning* (1990), *Carlson* (1991) ch. 12 and *Thorncroft et al.* (1993).

#### 3.1.1 *Horizontal distribution of frontal clouds*

An impression of the model's skill in predicting the horizontal distribution of the high clouds may be obtained from Figure 1. One can see from the 95% contour of the high cloud cover (HCC) in the model that the WCB associated cloudiness is correctly placed in the horizontal. However, the cross frontal extent of solid

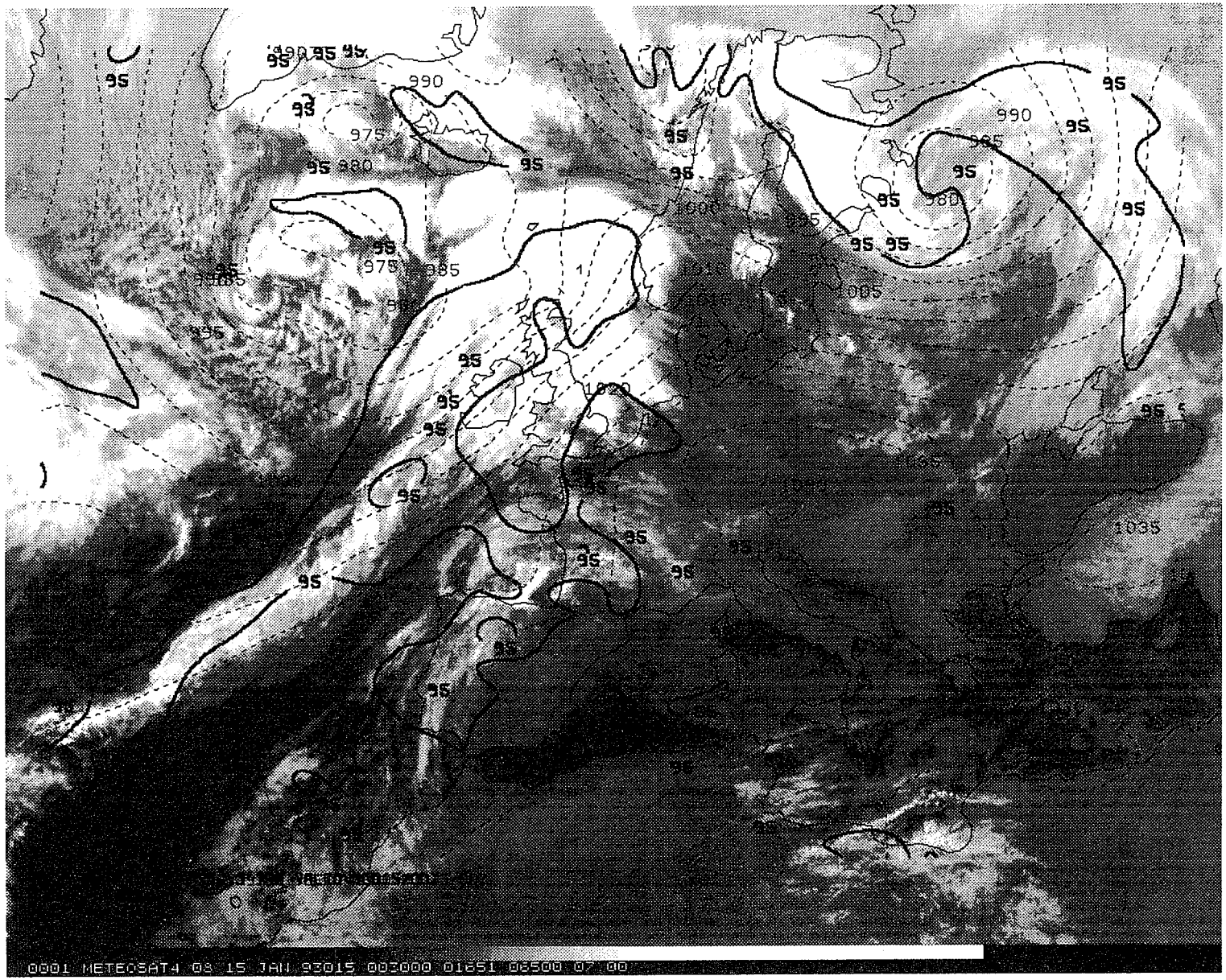


Fig. 1 Infrared (IR) METEOSAT imagery of Europe 15 January 00UTC. The heavy solid line is the 95% contour of the high cloud cover of the corresponding 36h forecast with the operational scheme. The thin dashed contours represent the forecasted mean sea level pressure (MSLP) in hPa at the same time.

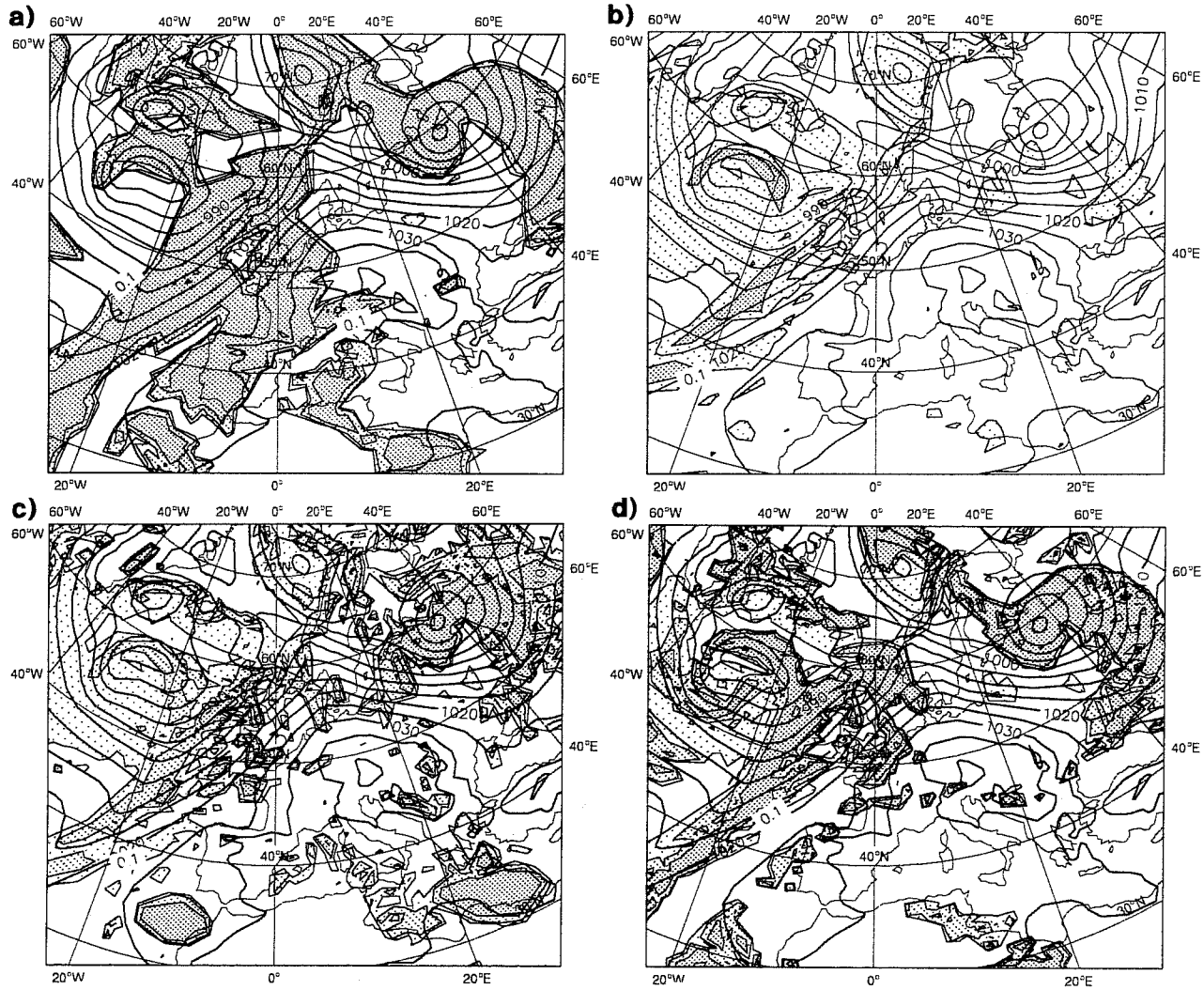


Fig.2 a) 36h prognosis of high cloud cover (HCC), with the operational scheme, valid 15 January 00UTC over Europe. Contour levels are 10%, 25% and 75%. The cloudiness field is overlaid the corresponding MSLP field. b) Same as a), but with convective cloud cover (CCC). Same as a), but with low cloud cover (LCC). d) Same as a), but with medium cloud cover (MCC).

high clouds is overestimated almost everywhere, except in the hammer head region. In this region it seems to be an underestimation of the horizontal extent of the cloudiness. This impression may be supported by plots such as Figure 1 and 2 throughout the periods.

As mentioned the CCB is often less extensive than the WCB. Following the conceptual cloud models of mid-latitude weather systems (See *Browning* (1990) and *Carlson* (1991)), clouds produced in the CCB may nearly always be associated with the occlusion, when seen in the horizontal plane. (The warm frontal part may often be hidden by the high clouds of the WCB). During the selected period, the model reproduces quite well the extent of the cloud belt on the occlusion, s. Figure 2.

A wave that enters the selected area about 15 January 12UTC is associated with a CCB starting just ahead of the WCB hammer head. However, as the leading surface ridge makes landfall (16 Jan. 12UTC) the imageries indicate that there are low level layered clouds along the warm front in the anticyclonic region. Both the relevant bias maps model output (not shown) show that most of these low level clouds are absent in the model.

The only period in which significant convection occurs over land is 15 January 06UTC to 16 January 00UTC over central Europe in connection with a warm front passage. The observers have reported alto cumulus (mid-level convection). The altocumulus clouds can be seen in Figure 1 over the North sea (a few hours before they make land fall). The corresponding CCC fields (e.g. Fig. 2c) indicate that the midlevel convection is absent in the model. Twelve hours later this deficiency can also be seen in the bias field over central Europe (Fig. 3).

### 3.1.2 *Vertical distribution of frontal clouds*

As mentioned, stratiform clouds are computed on the individual model levels. However, in the operational model the cloudiness fields are stored as Total Cloud Cover (TCC), High Cloud Cover (HCC) (450-100 hPa), Medium Cloud Cover (MCC) (800-450 hPa), Low Cloud Cover (LCC) (1000-800 hPa) and Convective Cloud Cover (CCC) during the postprocessing. During the selected period, the model fields (e.g. Fig. 2) show a rather general increase with height of the horizontal cross frontal extent of the cloud belts associated with the WCB. The model output also indicate that the fractional cloud amount increases with height, which implies that the lower clouds tend to be more broken than the fields aloft. Strictly one can not verify this model feature by the available "observations". Nevertheless, the infrared imagery indicate that the high cloud cover is quite broken equatorward of the "hammer head". Such an observation may be supported by the conceptual models, in which it is stated that cold dry air aloft is often crossing the WCB. The result is a potentially unstable lapse rate which may lead to convective clouds and a mixing of WCB air with that at higher levels. (When referring to the satellite imagery it is assumed that high clouds appear brighter than low clouds.)

### 3.2 Clouds in the northerly flow behind the cold front

#### 3.2.1 *Over sea*

Often midlatitude weather systems are associated with a rather extensive area of convective clouds over sea in the northerly flow behind the cold front. The dynamic structure of this flow is described by *Økland* (1983). There are several examples of this phenomenon occurring during the selected period (see Fig. 1). The areal extent of convective cloudiness regime is captured quite well by the model (see Fig. 2b), but both the imagery and ship observations indicate that the model rather systematically underestimates the fractional cloud amount (see Fig. 3). These clouds are reflected both in the MCC and LCC fields, which implies that the convection reaches above 800 hPa.

#### 3.2.2 *Over land*

As the cyclone makes landfall the characteristic cold air cumulus clouds disappear and are shortly replaced by low level layer clouds (see Fig. 1). Convective clouds may occur, but not in an organized manner, as over sea. The model produces some low clouds in relevant areas (see Fig. 2c), but the bias plots (Fig. 3) indicate that the forecasted cloud amount is too small.

### 3.3 Clouds in the anticyclone

During the first one or two days of the selected period, the satellite pictures (see Fig. 1) show a broken cloud belt stretching from the north west coast of Africa, along the Iberian west coast and eastward. Presumably that are the remainders of an old front that belonged to the low pressure system centred over Russia. By the 16 January 00UTC most of this cloud belt is evaporated. This cloud belt is represented by the model mostly as high clouds. (The images indicate that there may exist lower clouds as well, in reality.) The break up process is quite poorly reproduced by the model, which leads to an overestimation of the cloud cover in this region 15 to 16 January. (see Figs. 2a). The maximum error is located west of the Gibraltar strait. More or less the same situation is occurring 18 January. The model is not able to sufficiently break up the clouds of a front that has become inactive/passive. The error seems to be most pronounced in the upper layers.

The satellite pictures show that large areas in the western parts of the Mediterranean sea are covered with low layer clouds (maybe fog) during most of the period. The model outputs and synop observation shows that those clouds are systematically underestimated in the model, both with respect to horizontal extent and fractional cloud cover amount.

In the February case a high is centred over Russia. As for the January case the operational cloud scheme underestimates the low clouds in this regime. An exception is areas in which the model atmosphere has an unrealistic strong low level inversion. Here the predicted cloud amount is far too high.

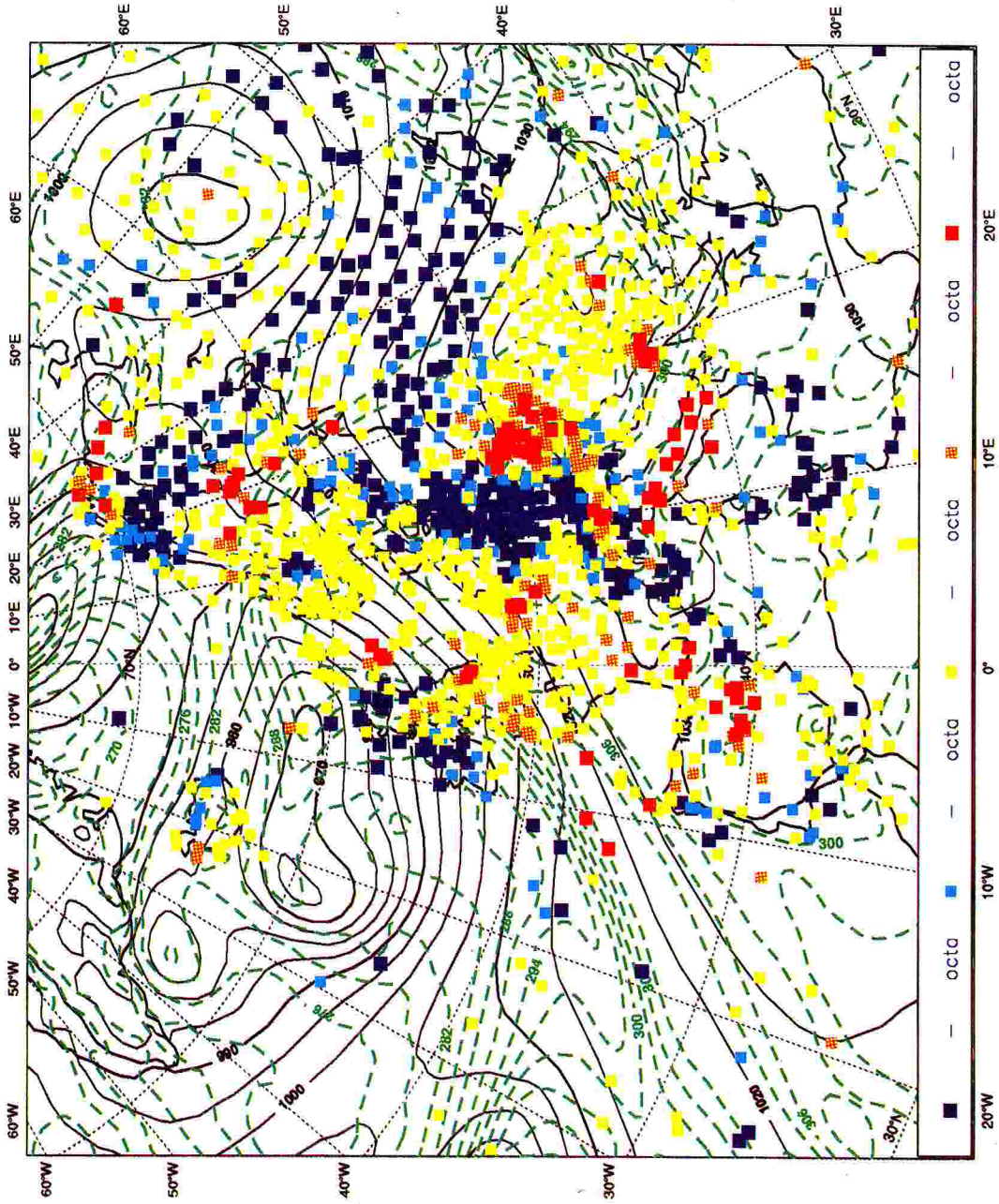


Fig.3 Difference between 48h predicted total cloud cover (TCC), valid at 15 January 12UTC over Europe, and surface observed $TCC_{obs}$ at the same time. TCC is predicted with the operational scheme. The difference (or bias) field, Δ, is separated into 5 octa intervals, each with a different colour: $-8 \le \Delta < -4$ navy blue, $-4 \le \Delta < -2$ light blue , $-2 \le \Delta \le 2$ yellow, $2 < \Delta \le 4$ orange and $2 < \Delta \le 4$ red. The green dashed contours are the equivalent potential temperature field ate 850hPa. The black solid contours are the mean sea level pressure field (in hPa).

## 4. RESULTS FROM RUNS WITH THE NEW SCHEME

Another set of forecasts (for the same period) have been carried out with the ECMWF model, in which the operational cloud scheme has been replaced by the new cloud scheme.

### 4.1 Horizontal distribution of frontal clouds

The over all impression is that the frontal clouds are quite well reproduced with the new scheme. Several detailed patterns are reflected in the model. However, there are deficiencies. The most apparent and systematic one is an underestimation of the high cloudiness in the occlusion and "hammer head" regions (see Fig. 4). It would be interesting to see if this deficiency would be reduced if advection of the specific cloud mass were included in the experiments with the new scheme.

Like the operational scheme, the new scheme also seems to underestimate the low layer cloud extent along the warm front (see Fig. 5 and 6), but to a far lesser degree than the operational scheme.

The previously mentioned midlevel convection (see section 3.1.1) that took place over central Europe 15-16 January is not forecasted by the new scheme either (See Figs. 4, 5 and 6).

From the 16 Jan 18UTC and onwards the new scheme overestimates the HCC and LCC in the poleward part of the warm sector.

### 4.2 Vertical distribution of frontal cloudiness

The model output (Fig. 5) shows that there is no systematic trend in the variation of cloud extent and fraction with pressure. On the contrary, the conveyor belt clouds seem to have small variations between cloud top and cloud base. For the equatorward part of the WCB this seems to be well in agreement with conceptual models, but in the "hammer head" region one should expect a decrease of cloud extent with pressure. Note that areas with a $< 95\%$ constitute the major part of HCC.

### 4.3 Clouds in the northerly flow behind the cold front

The new scheme seems to represent the observed cloudiness in this region quite well, both over land and sea. As for the operational scheme, the convective cloudiness is reflected both in MCC and LCC (see Fig. 5).

### 4.4 Cloudiness in the anticyclone

The previously commented (Section 3.3) inactive front in the first part of the selected period is associated with clouds that evaporate in a 18h period during the 15-16 Jan. The evaporation process seem to take place in the model but the intensity is too weak, which leads to an overestimation of the cloudiness over the Iberian west coast. Comparing the forecasts done with the new and the operational scheme it is apparent that this cloudiness is more broken in the "new scheme" forecasts than in the operational ones.

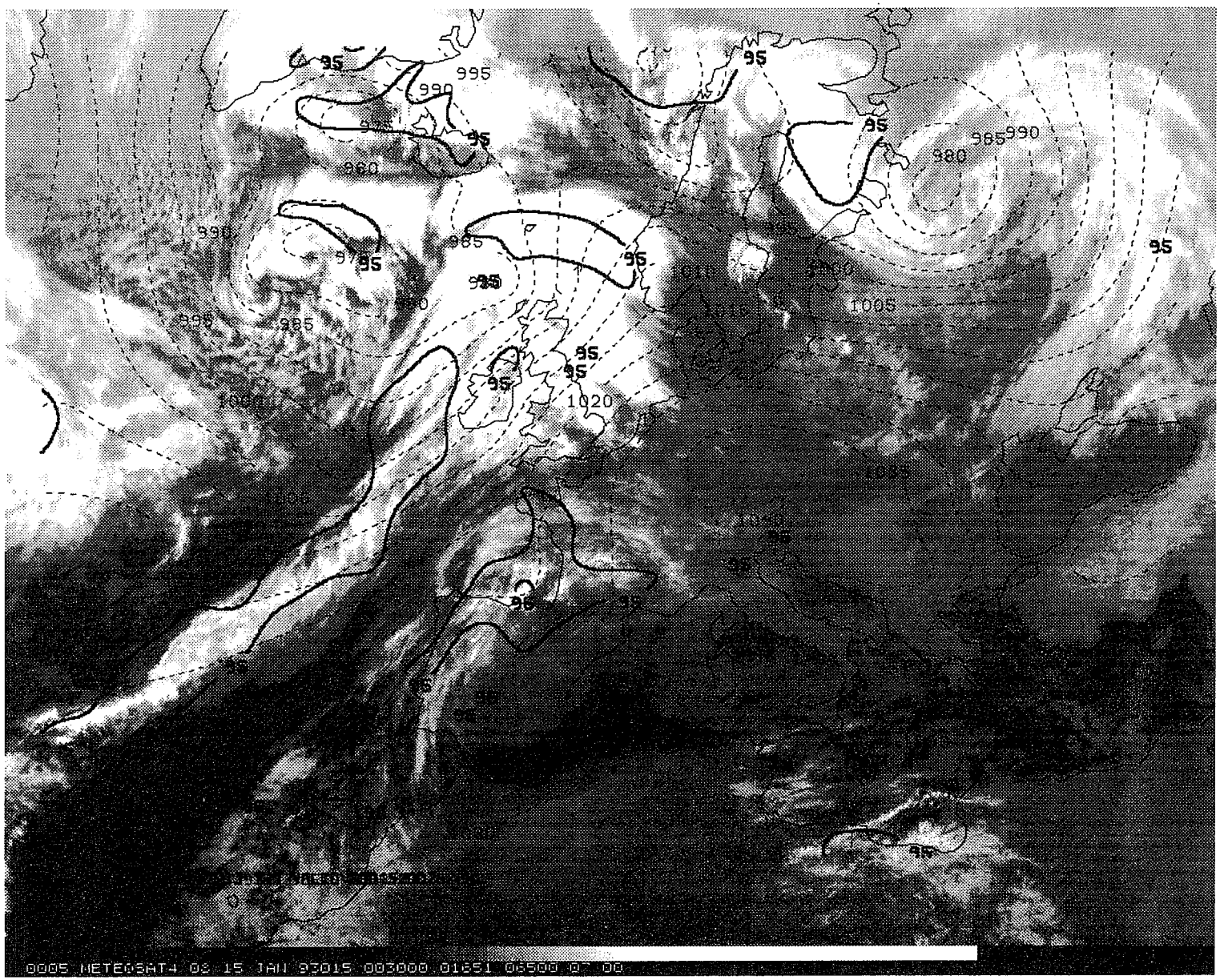


Fig.4 Same as 1, but the HCC forecast is done with the new cloud scheme.

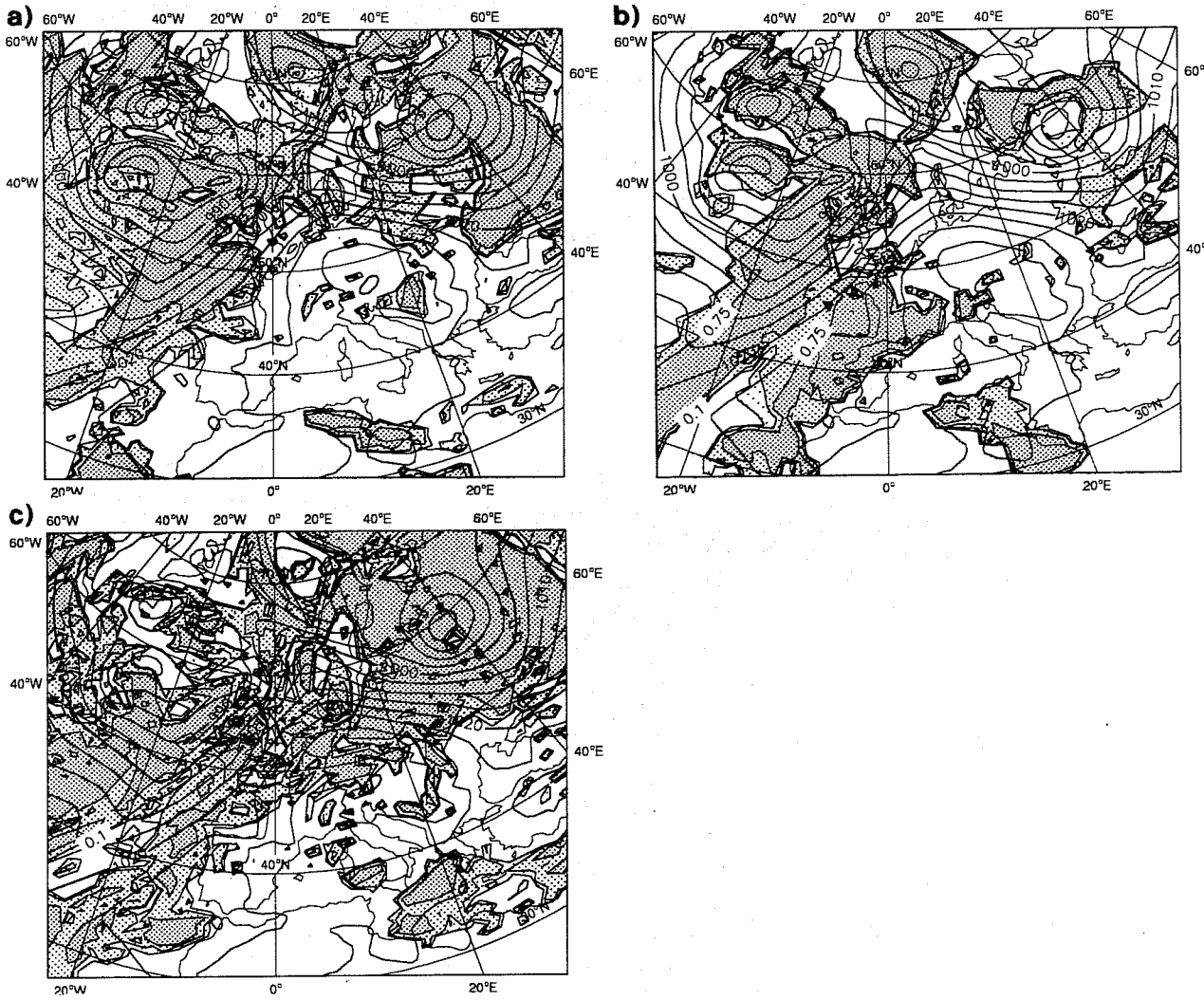


Fig.5 Same as 2 except that the cloudiness forecast is done with the new cloud scheme. a) MCC, b) HCC, c) LCC. Note that the new scheme does not distinguish between convective and stratiform cloudiness, which is why CCC is absent here.

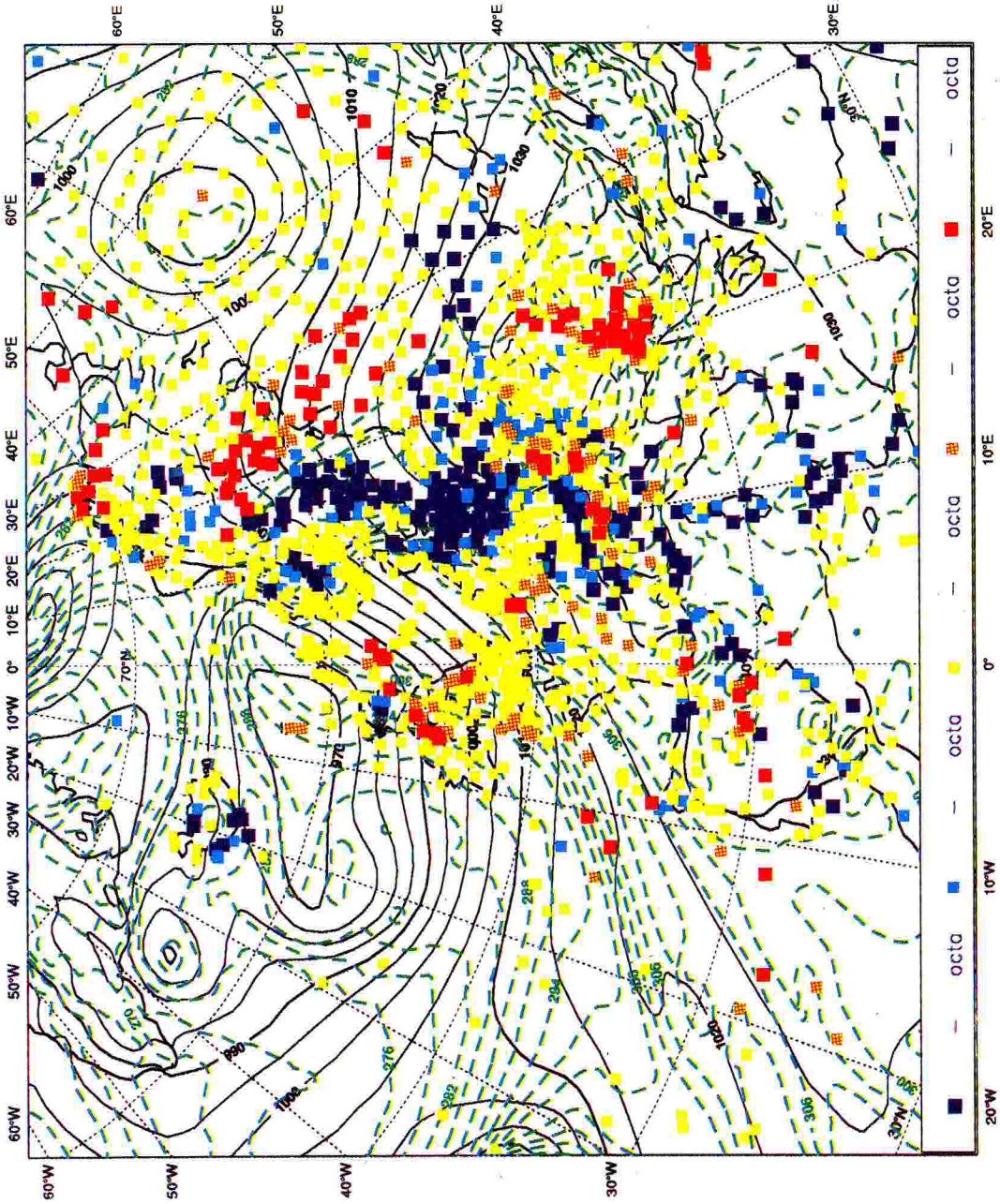


Fig. 6 Same as 3 except that the cloudiness forecast is done with the new cloud scheme.

As for the operational scheme, the low layer clouds/fog in the Mediterranean sea is systematically under represented here as well, however not to the same extent. The new scheme is also associated with spurious clouds in the unrealistic thermal states that occurred in the February case.

## 5. STATISTICS

A more quantitative intercomparison between the model output and the synop observations is listed in this section. Figure 7 a) to c) show that with respect to area averaged bias, standard deviation and correlation coefficient, the new scheme compares favourably with the operational scheme. The diurnal variation in Figure 7 a) is merely due to the fact that it is difficult for the observer to discover clouds at night. This underlines that it is the local noon observation that is most reliable.

The absolute cloud frequency diagrams in Fig. 8a and b show that the operational scheme has a tendency to produce too often a fractional cloud cover value between 0 and 2 octas and underestimates the occurrence of overcast condition. The opposite error occurs in the 2 upper intervals. The same error pattern may be found for the new cloud scheme. However, the absolute error values are smaller here. Such diagrams give only information of frequency distribution within each data set. To obtain the number of points in each octa class that corresponds to the same class in the observed data set, one can calculate the surface and/or contour the cross frequency matrix. Such surface/contour plots are contained in Fig 9. From both Fig 9a and 9b one can clearly see that both schemes have forecasted points in the "wrong corners" of the diagram. In order to identify the flow type that might be associated with the points most distant from the (0,0) -(8,8) diagonal, one may split the data into different flow classes. One example/suggestion is given in Fig 9c and d where forecasts with the "new scheme" of cloud frequency vs observed cloud frequency is split into one anticyclonic class and one cyclonic class. (The relative vorticity at 850hPa is taken as the criterion). It is evident from Fig 9c that the majority of the cyclonic points have an observed cloud cover above 5 octas, whereas the forecasted cloud fraction covers the full range. Even though phase errors in the forecast and observation errors may cause spread in such diagrams, it is worth exploring the potential of this method.

The cloudiness bias frequency distribution may also be suggestive with respect to diagnosing forecast errors. The bias distributions for both schemes averaged over four 48h forecasts (15 - 19 Jan.) are plotted in Fig. 10. Except for the right hand tail, the new scheme is associated with a smaller amount of biases than the operational scheme. However, both cloudiness forecasts have the same distribution shape with three maxima. Some of the characteristics of the points in the tails of the bias distribution may be seen in Fig. 11. The points which have bias > 5 octas (overestimated cloud amount), seems to be mostly low clouds (60%) in the new scheme case, whereas the operational scheme overestimates both high and low clouds. This difference between the two schemes is also reflected in the more subjective assessment of the two cloudiness forecasts.

In the opposite tail of the bias distribution it is observed low cloud base in most of the points where the both schemes have underestimated the cloud amount by more than 5 octas (see Fig. 12). One should be aware that the lowest significant clouds not necessarily constitute the dominant cloudy area. However, Fig 13 shows

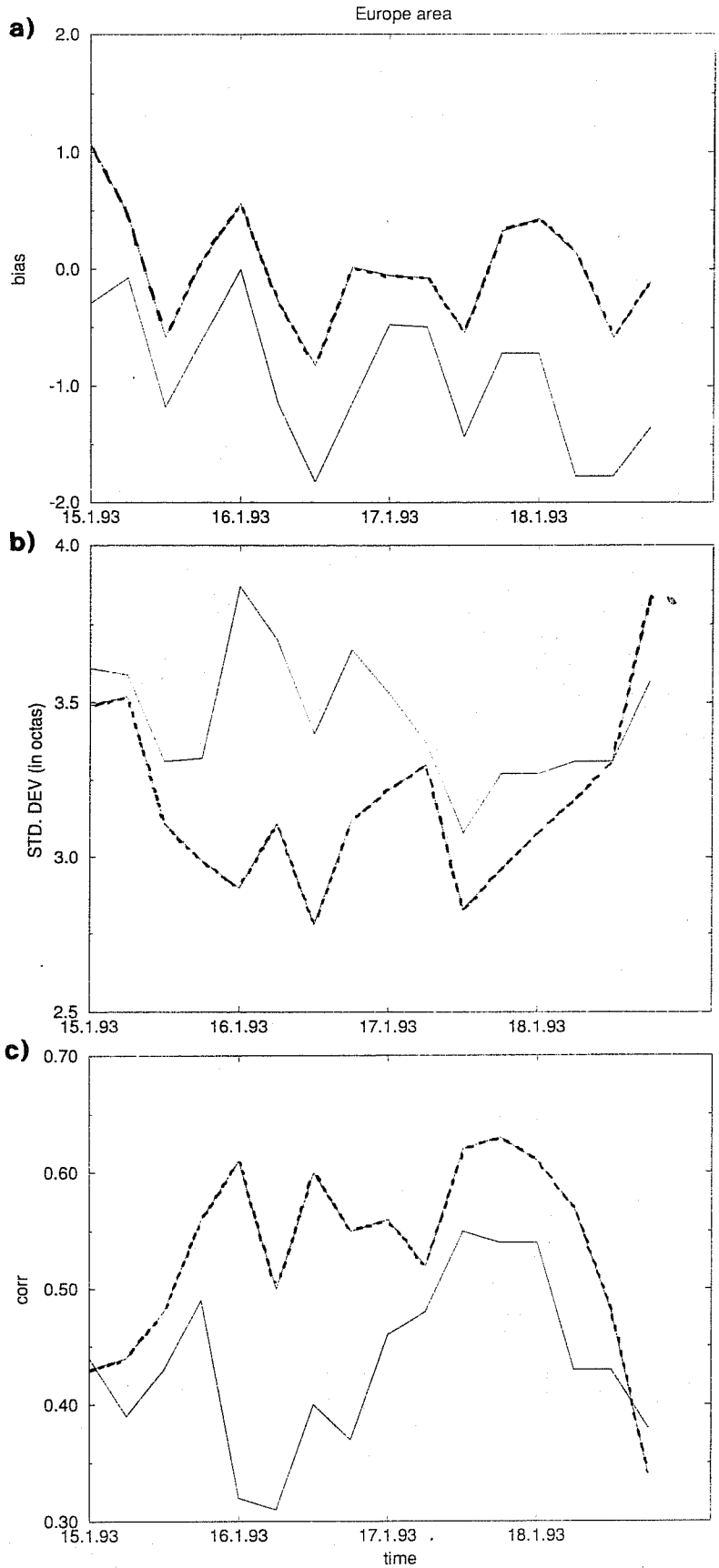


Fig.7 a) Averaged differences (bias) between forecasted and surface observed fractional cloud cover (in octas). The solid and dashed lines represent biases calculated on basis of cloud cover produced by the operational and new scheme, respectively. The horizontal axis in the diagram represents the verification time (each day at 00UTC is tic-marked). The four observation times each day (0, 6, 12 and 18UTC) verify the 36h, 42h, 48h and 54h forecasts, respectively. b) Same as a), except that the curves represent averaged standard deviation. c) Same as a), except that the curves represent averaged correlation coefficient.

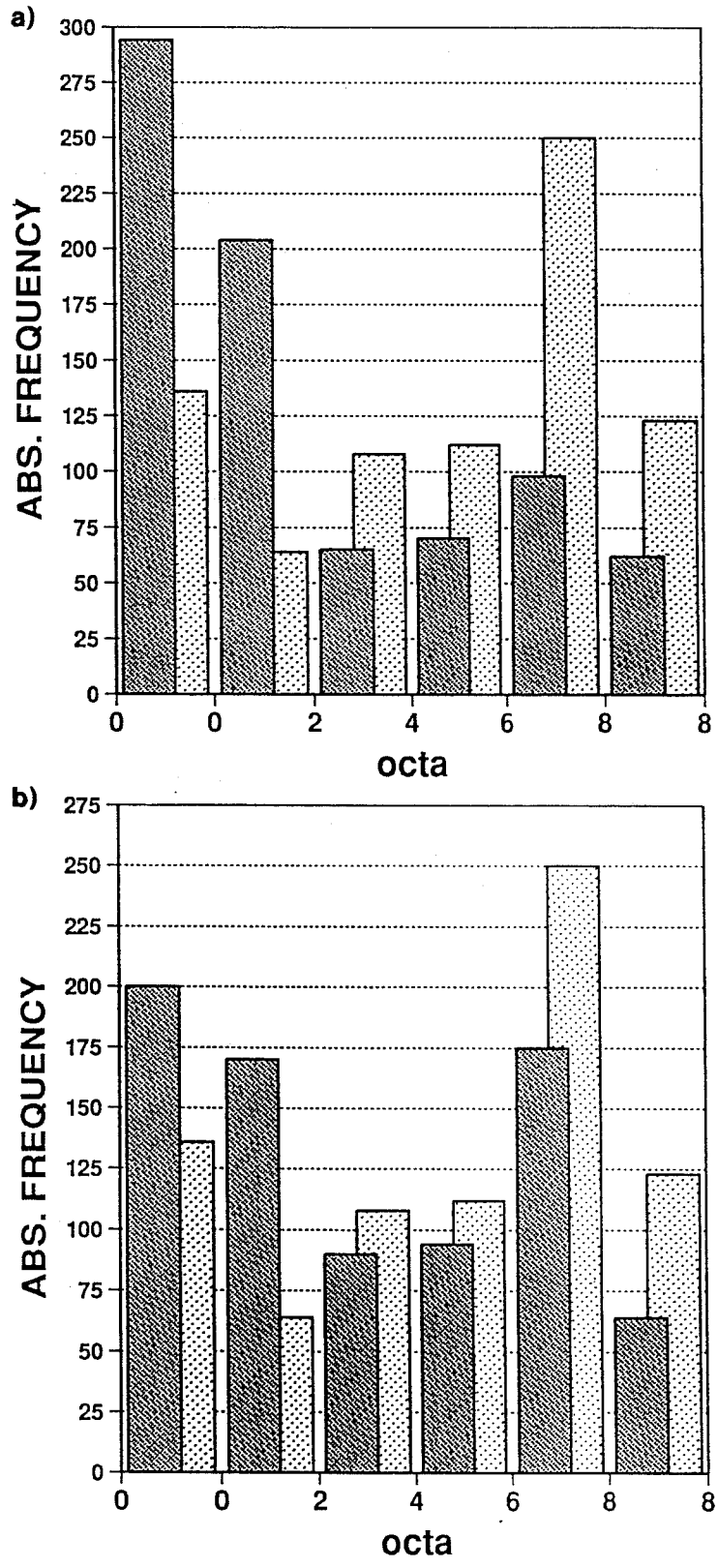


Fig.8 a) Light shaded columns are frequency distribution of the surface observed fractional cloud cover (in octas) over Europe. The heavy shaded columns are the fractional cloud cover from a 48h forecast with the operational scheme. Observation time is 16 January 12UTC. b) Same a), but the forecast is done with the new scheme.

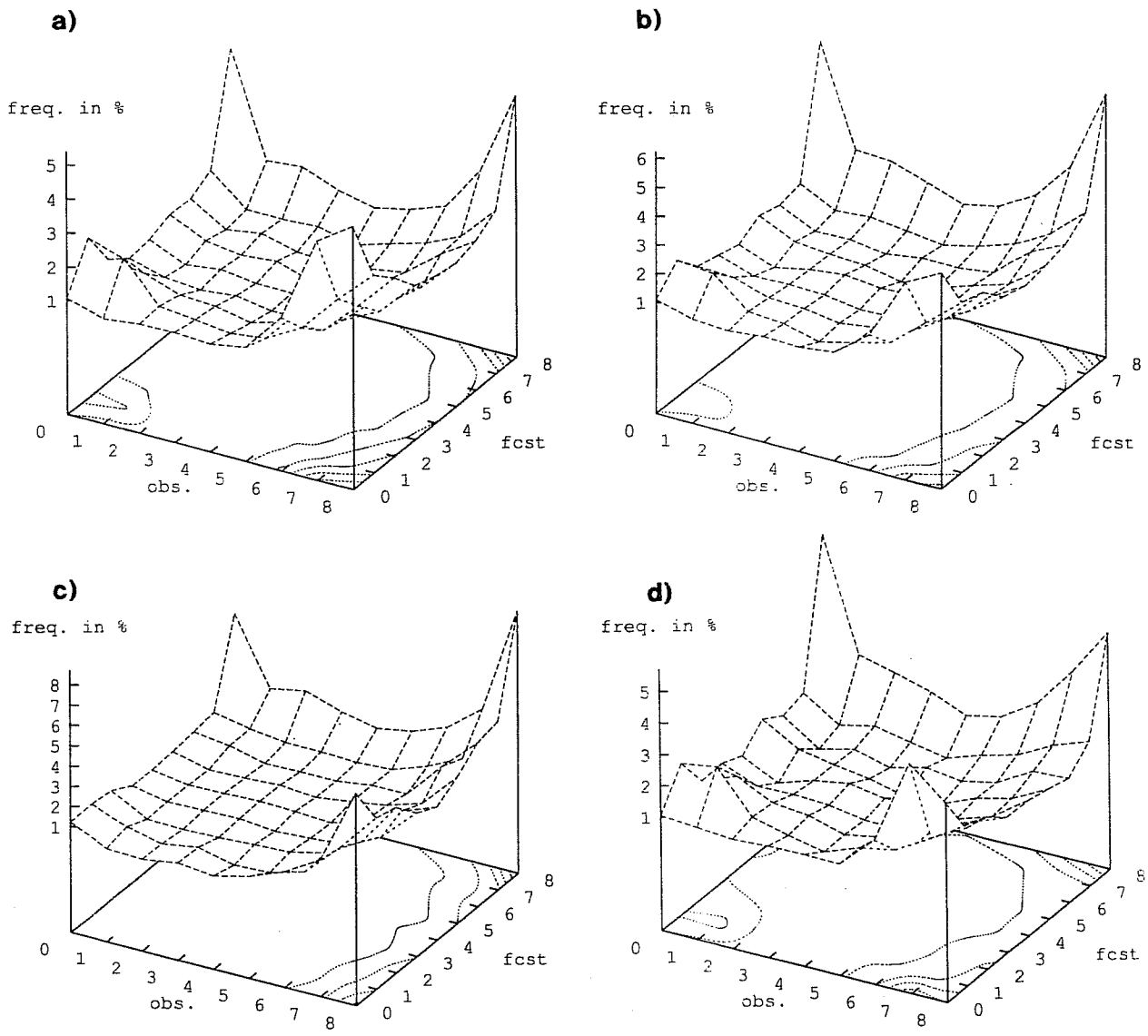


Fig.9 a) Surface and contour representation of the cross frequency matrix. The observed and forecasted cloudiness values are set along the horizontal axes and the frequency (in %) is set along the vertical axis. The forecasted frequencies are the average of the 48h forecasts in the period 15-18 January 1993. The observed frequencies are the average of the 12UTC observations in the same period. b) Same as a), but the forecasts are done with the new scheme. c) Same as b), but the matrix contains cyclonic points only. (A point is cyclonic if the relative vorticity at 850hPa is greater than zero.) d) Same as b), but the matrix contains anticyclonic points only.

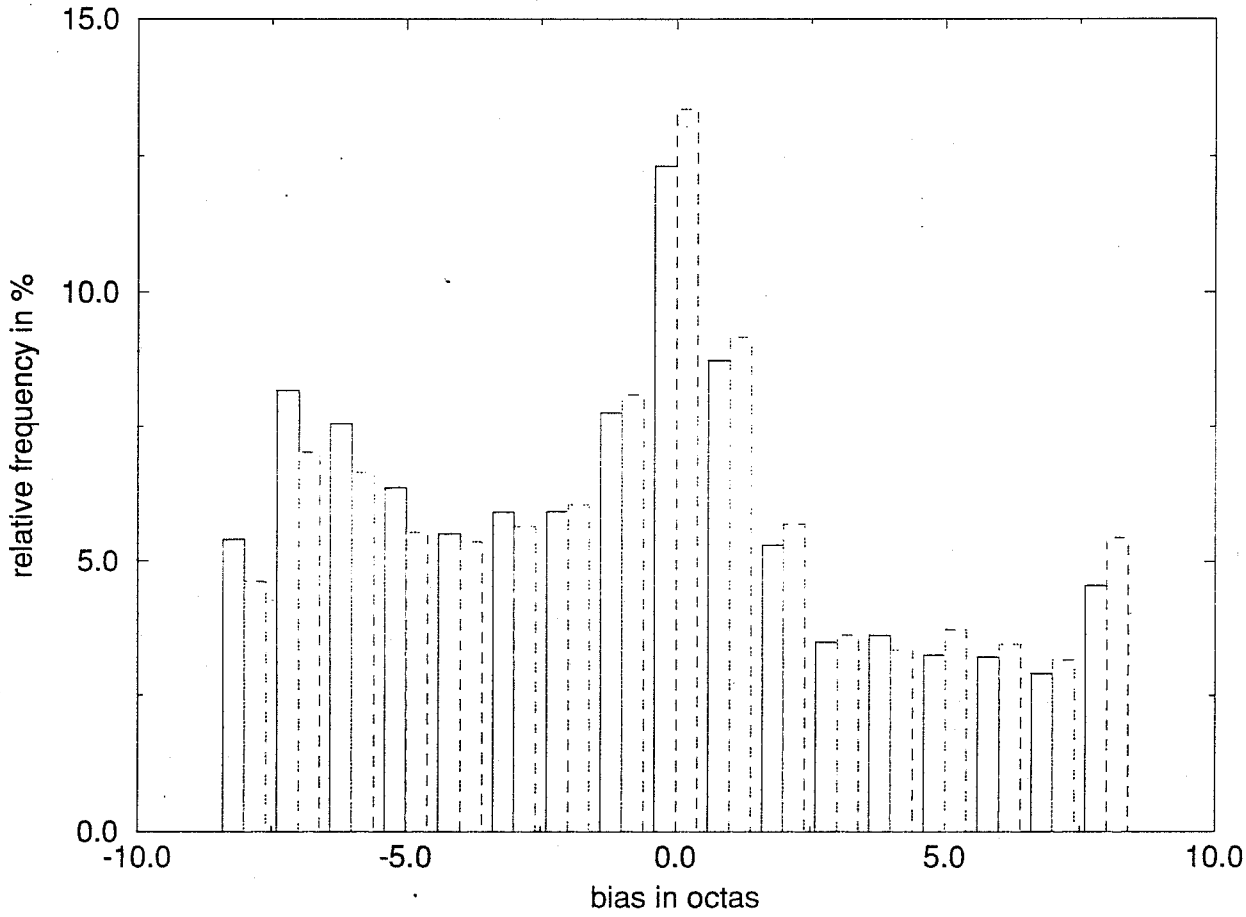


Fig.10 Cloud bias frequency distribution averaged over the 48h forecasts in the 15-18 January 1993 period (Bias = forecasted cloud fraction - observed cloud fraction). The solid bars are the distribution obtained from the operational forecast. The dashed bars are the distribution obtained from the "new scheme" forecasts.

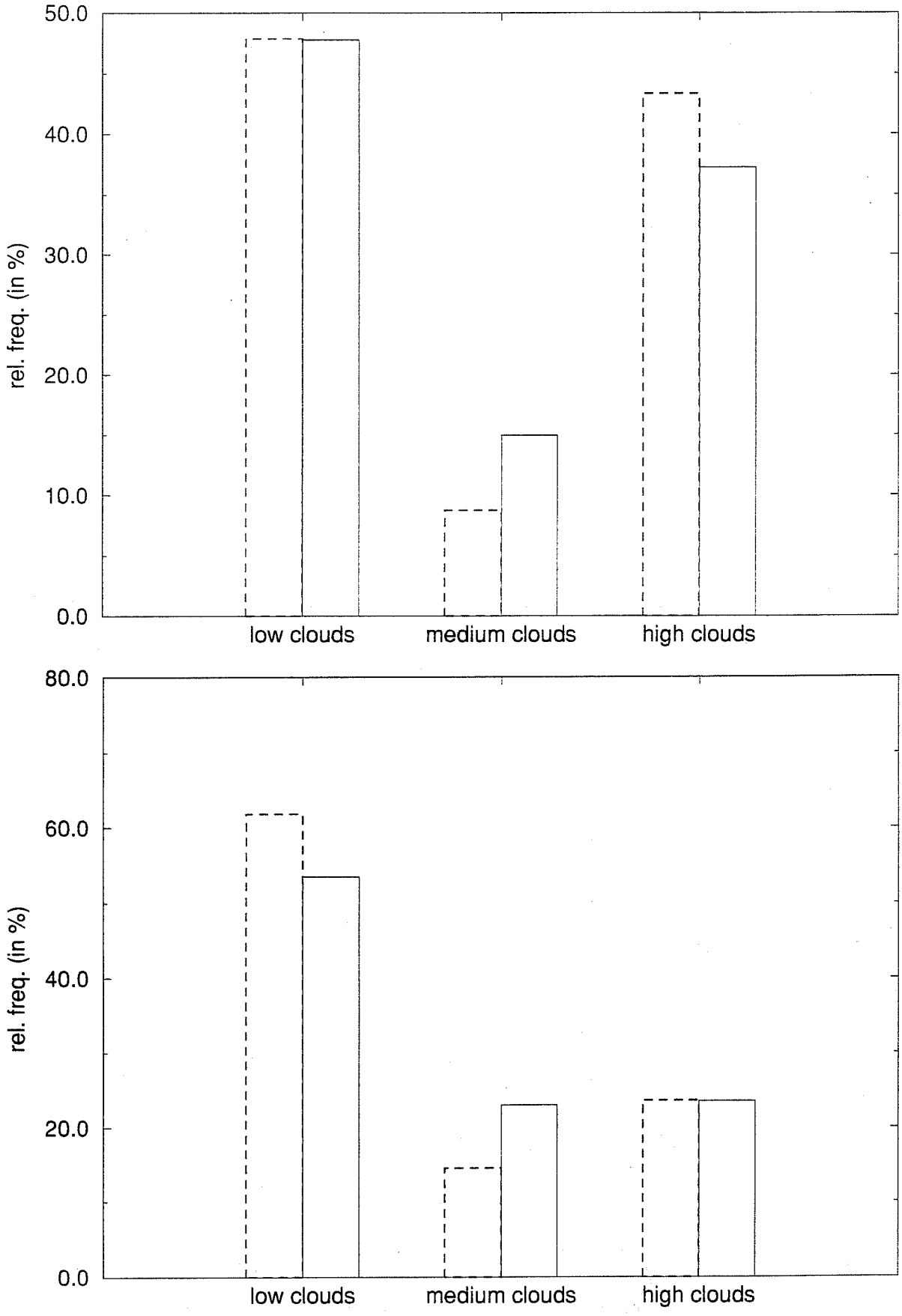


Fig.11 a) Solid bars: Forecasted cloud layer distribution for biases with value greater than 5 octas. Dashed bars: Dominating cloud layer distribution of biases with value greater than 5 octas. (The dominant cloud layer in a column is the one with largest cloud fraction.) Both distributions are the averages over the 48h operational forecasts in the 15-18 January period. The three cloud layers are: Low clouds (1000 - 800hPa), medium clouds (800 - 450hPa) and high clouds (450 - 100hPa). b) Same as a), but the forecasts are done with the new scheme.

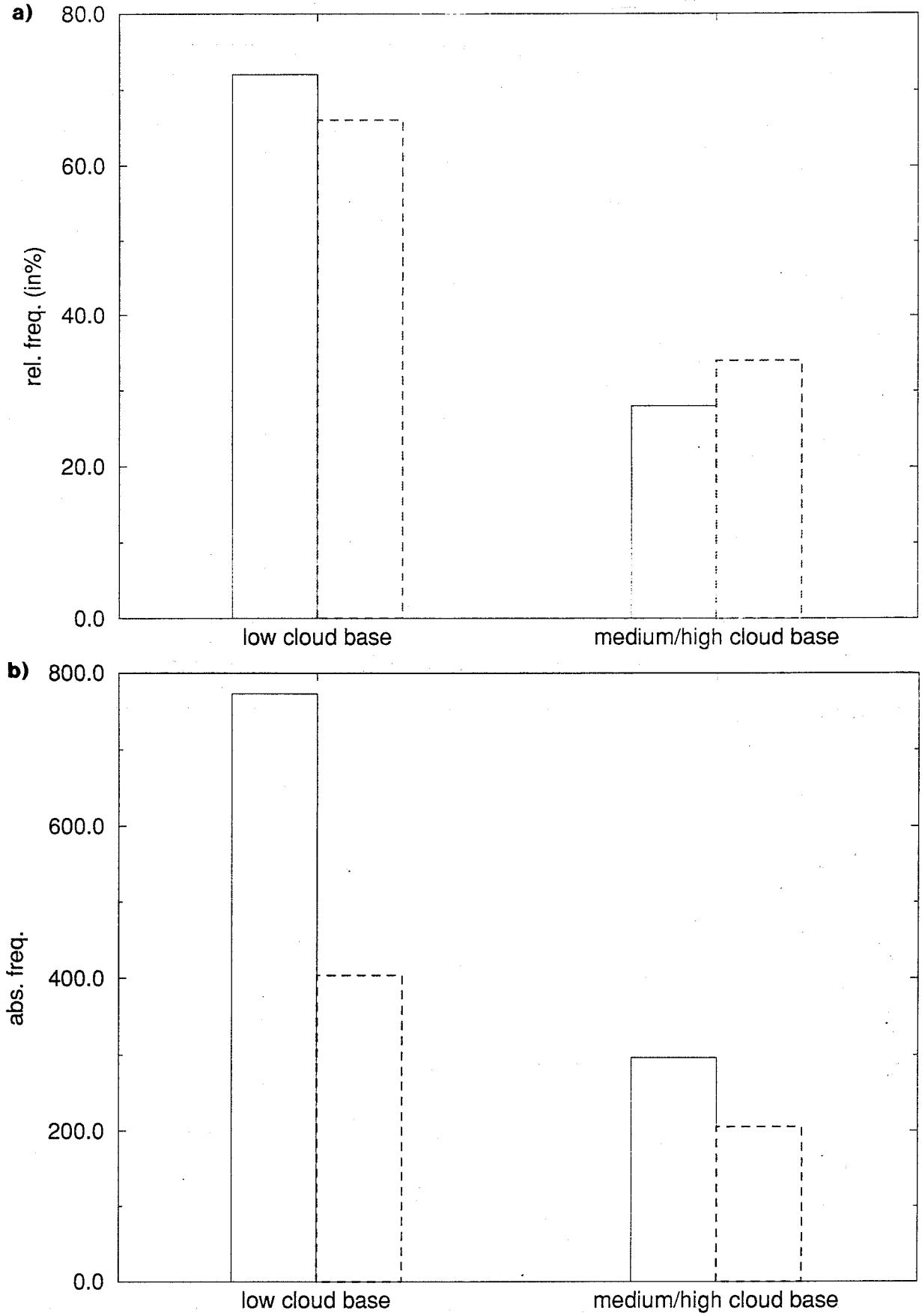


Fig.12 a) Solid bars: Observed cloud base height distribution, averaged over the 12UTC observations in the 15-18 January 1993 period, for biases with value less than -5 octas. The biases are calculated on basis of the operational forecast. Dashed bars: Same as solid bars, but for biases calculated on basis of forecasts with the new scheme. The observed cloud base height of the lowest significant cloud layer is divided into two classes: Low clouds (base height less than 1900m ) and high clouds (cloud base greater than 1900m). b) Same as a), but with absolute frequency along the vertical axis.

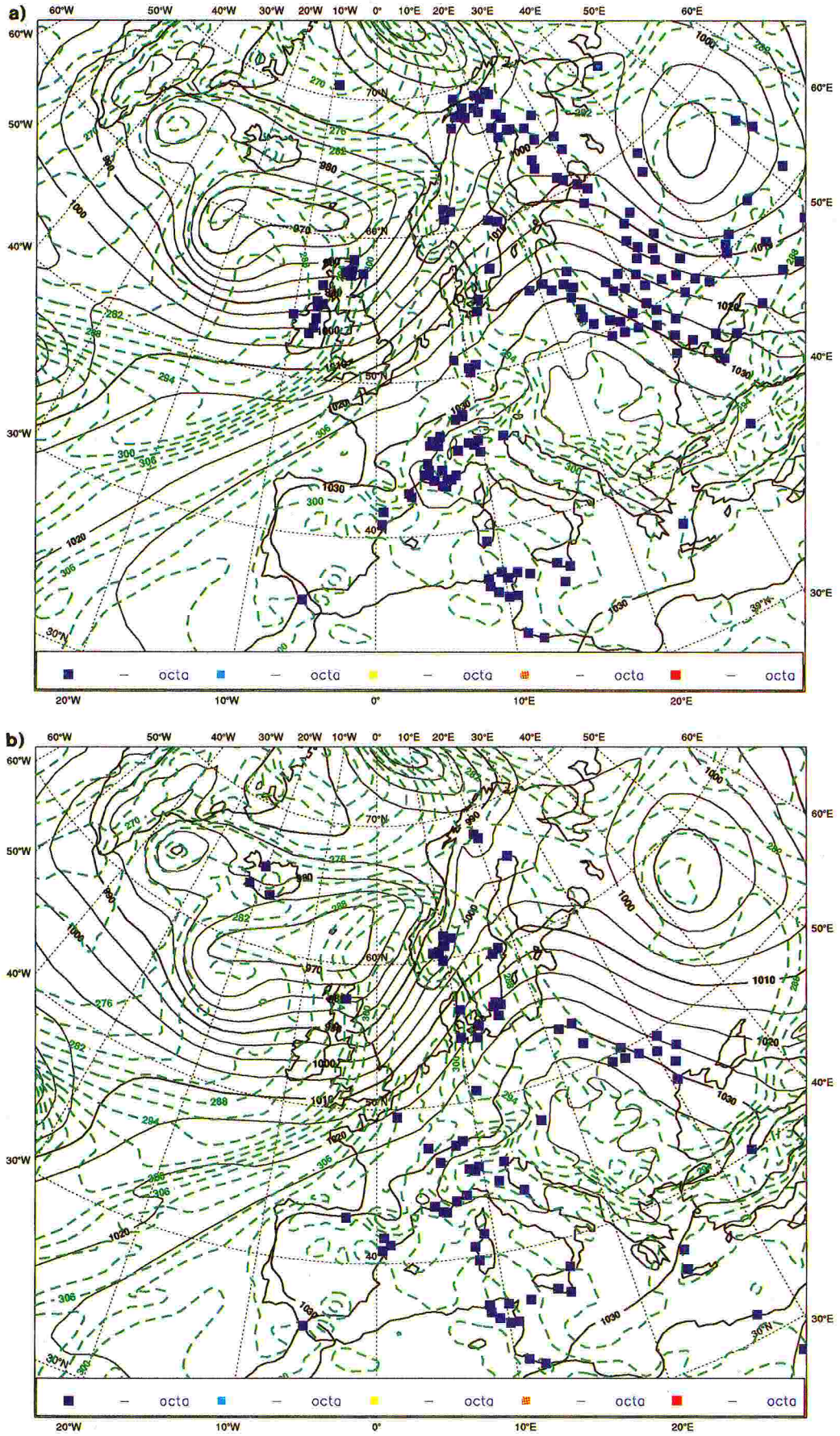


Fig.13 a) Same as 3, but only biases with value less than -5, with observed low cloud base are included. b) Same as a), but the forecasts are done with the new scheme.

where those points are situated in the flow. This example shows clearly that the new scheme has improved the representation of low clouds behind the cold front over land. In order to have confidence in such an identification, the amount of investigated data need to be larger than in this example, both with respect to sampling time and area domain.

## 6. SUMMARY

Short range cloudiness forecasts (36-72h) with the operational ECMWF cloud scheme (*Slingo*, 1987) and a new scheme (*Tiedtke*, 1993) have been validated in two winter cases over Europe. The two periods are 15 - 18 January 1993 and 14 February 1993. The forecasted cloud fields have been compared with cloud structures in METEOSAT IR imageries, surface synop observations and conceptual models. The skill of the operational scheme may me summarized in Table 1 below. The new scheme has improved the deficiencies of the operational cloudiness forecast in nearly all the cloud regimes contained in Table 1. The only exception is that the high cloudiness in the hammer head is systematically underestimated here as well.

| **Cloud regime** | **Horizontal distribution of cloudiness** | **Vertical distribution of cloudiness** |
|---|---|---|
| Cold front | Realistic, but overestimated cloud fraction in the upper layers | Cloud amount increases with height |
| Behind the cold front | Underestimated, both over land and sea | Mostly low clouds |
| Warm front | Underestimated | Mostly low clouds |
| Occlusion and hammer head region | Realistic in occlusion, but underestimated in the upper hammer head region | |
| Anticyclone | Underestimation of low clouds. Spurious low clouds over land due to unrealistic inversions. Overestimation of clouds associated with interactive cold fronts. | |

Table 1: Summary of the performance of the cloudiness forecast with the operational ECMWF scheme for two winter cases

Acknowledgements

I thank Dr. G. Kelly for supplying and helping me with useful software. The assistance given by Dr. A. Lanzinger is also gratefully acknowledged.

References

Browning, K.A., 1990. Organization of clouds and precipitation in extratropical cyclones. The Eric Palmén memorial volume. American Meteorological Society, Boston.

Carlson, T.N., 1991. Mid-Latitude Weather Systems. Harper Collins Academic. 77-85 Fulham Palace Rd., Hammersmith, London W6 8JB, UK

Morcrette, J.-J., L. Illari, E. Klinker, H. LeTreut, M. Miller, P. Rash, and M. Tiedtke, 1991. Clouds and Radiation in the ECMWF model - Recent Developments. ECMWF Technical Memo. n 181, Reading, U.K., 48pp.

Slingo, J.M., 1987. The development and verification of a cloud prediction scheme in the ECMWF model. Quart.J.Roy.Meteor.Soc. 113, 899-927.

Thorncroft, C.D., B.J. Hoskins and M.E. McIntyre, 1993. Two paradigms of baroclinic-wave life-cycle behaviour. Quart.J. Roy.Meteor.Soc. 119, 17-55.

Tiedtke, M., 1993. Representation of Clouds in Large-Scale Models. Accepted for publication in Mon.Wea.Rev.

Økland, H., 1983. Modelling the height, temperature and relative humidity of a well-mixed planetary boundary layer over a water surface. Boundary-Layer Meteorology 25 121-141.